Journal of Alloys and Compounds 502 (2010) 87–91

Contents lists available at ScienceDirect

Journal of Alloys and Compounds

journal homepage: www.elsevier.com/locate/jallcom

# Isothermal section of the Y–Fe–Cr ternary system at 773 K

Wei He*, Xiaohua Wang, Jinman He, Jingxian Wen, Meihua Yu, Lingmin Zeng

*Key Laboratory of Nonferrous Metal Materials and New Processing Technology, College of Materials Science and Engineering, Ministry of Education (Guangxi University), Nanning 530004, PR China*

ARTICLE INFO

*Article history:*
Received 24 January 2010
Received in revised form 19 April 2010
Accepted 23 April 2010
Available online 4 May 2010

*Keywords:*
Phase diagram
Y–Fe–Cr system
X-ray diffraction

ABSTRACT

The isothermal section of the phase diagram of the Y–Fe–Cr ternary system at 773 K was investigated by X-ray powder diffraction (XRD), optical microscopy, differential thermal analysis (DTA), scanning electron microscopy (SEM) equipped with energy dispersive spectroscopy (EDS). The isothermal section consists of 8 single-phase regions, 14 two-phase regions and 7 three-phase regions. The maximum solid solubilities of Cr in Fe, $Y_2Fe_{17}$, $Y_6Fe_{23}$ and $YFe_2$ are 13, 18, 6 and 6 at.% Cr, respectively. The maximum solid solubility of Fe in Cr is about 15 at.% Fe. It was found that there is some homogeneity range in the ternary compound of $YFe_{12-x}Cr_x$ with $x = 2.1–3.4$ at 773 K.



## 1. Introduction

Rare-earth iron-rich intermetallic compounds formed in many R–Fe–M (R is rare-earth element, M is transition metal) system exhibit excellent magnetic properties. The magnetic properties of the ternary compounds of $R(Fe,M)_{12}$ and $R_3(Fe,M)_{29}$ have been investigated intensively [1–15]. In both the compounds, the presence of a third element M (M = Ti, V, Cr, Mn, Nb, Mo, W, etc.) is necessary for the stabilization of the two phases. These compounds are considered as potential permanent magnet materials due to their fairly high values of the Curie temperature, saturation magnetization and magnetocrystalline anisotropy. The inherent magnetic properties of these compounds can be further improved by introducing nitrogen, carbon or hydrogen in the interstitial positions [16–19].

The phase diagrams of Y–Fe, Y–Cr and Fe–Cr binary systems are reported in Ref. [20]. There are four compounds, i.e. $Y_2Fe_{17}$, $Y_6Fe_{23}$, $YFe_3$ and $YFe_2$ existing in the Y–Fe binary system. Two investigations on the phase diagram of the Fe–Cr system were found in literature [21,22]. It was reported that there is a unique binary compound FeCr (σ phase) in the Fe–Cr system. Kubaschewski [21] suggested that the σ phase existed at the temperatures below 1103 K, while Itkin [22] considered that the σ phase existed above 713 K and pointed that the top of the miscibility gap was about 818 K. No binary compound was found to exist in the Y–Cr system according to Ref. [20]. Two ternary compound of the Y–Fe–Cr system, i.e. $YFe_{10}Cr_2$ and $Y_3(Fe,Cr)_{29}$ have been found in literature [2,9,10]. Investigations on the compound $YFe_{10}Cr_2$ were available in Refs. [2,9]. The phases of $Y_2Fe_{17}$ (with $Th_2Ni_{17}$-type structure), $YFe_{10}Cr_2$ (with $ThMn_{12}$-type structure) and $Y_3(Fe,Cr)_{29}$ (with $Nd_3(Fe,Ti)_{29}$-type structure) can be derived from the basic hexagonal $CaCu_5$-type structure by the replacement of 1/3, 1/2 and 2/5 of the Y atoms by a pair of Fe atoms (known as dumb-bell atoms), where Y and Fe occupy the Ca and Cu sites, respectively. The crystallographic data of the binary and ternary compounds in the Y–Fe–Cr system are listed in Table 1. However, the investigation on the phase relationships of the Y–Fe–Cr ternary system is not available in literature. The purpose of this work is to investigate the phase relations of the Y–Fe–Cr ternary system at 773 K.

## 2. Experimental

A total of 188 alloy buttons with weight of 2 g each were prepared in an electric arc furnace under argon atmosphere using a water-cooled cooper crucible. The purities of Y, Fe and Cr were 99.9 wt.%, 99.99 wt.% and 99.9 wt.%, respectively. Titanium was used as an oxygen getter during the melting process. The alloy buttons were re-melted three times to ensure homogeneity. The weight losses of most alloys were less than 1% after melting. All the as-cast samples were sealed in evacuated quartz tubes for homogenization annealing. The heat treatment temperatures were chosen according to the results of differential thermal analysis (DTA) on some typical alloys or based on previous work of the binary systems. The Fe-rich or Cr-rich alloys were kept at 1173 K for 30 days for homogenization, while the other alloys homogenized at 973 K for 30 days. After that, all the alloys were cooled down to 773 K at a rate of 50 K/day and then kept for at least 10 days and finally quenched into liquid nitrogen.

The X-ray diffraction (XRD) data were collected on a Rigaku D/Max 2500V diffractometer with Cu $K_\alpha$ ($\lambda = 0.154056$ nm) radiation and graphite monochromator operated at 40 kV, 200 mA. Data for Rietveld refinement were collected in the $2\theta$ range from 15° to 100° with a step size of 0.02° and a counting time of 2 s per step. The Materials Data Inc. software Jade 5.0 [24] with powder diffraction file (PDF release 2002) was applied for the phase identification. The differential thermal analysis (DTA) was performed on a Netzsch STA 409PC thermal analyzer. The Hitachi S-3400N scanning electron microscopy (SEM) equipped with EDAX energy

* Corresponding author. Tel.: +86 771 327 5918; fax: +86 771 323 9406.
*E-mail addresses:* elsawh@126.com, wei_he@gxu.edu.cn (W. He).

0925-8388/$ – see front matter © 2010 Elsevier B.V. All rights reserved.
doi:10.1016/j.jallcom.2010.04.161

**Table 1**
Crystal structure data of the binary and ternary compounds in the Y–Fe–Cr system.

| Compounds | Space group | Structure type | Lattice parameters (nm) | | | | Refs. |
|---|---|---|---|---|---|---|---|
| | | | *a* | *b* | *c* | *β* | |
| FeCr | $P4_2/mnm$ (No. 136) | FeCr | 0.87966 | – | 0.45582 | | [23] |
| $Y_2Fe_{17}$ | $P6_3/mmc$ (No. 194) | $Th_2Ni_{17}$ | 0.8472 | – | 0.8288 | | [23] |
| $Y_6Fe_{23}$ | $Fm\bar{3}m$ (No. 225) | $Th_6Mn_{23}$ | 1.212 | – | – | | [23] |
| $YFe_3$ | $R\bar{3}m$ (No. 166) | $NbBe_3$ | 0.5139 | – | 2.459 | | [23] |
| $YFe_2$ | $Fd\bar{3}m$ (No. 227) | $MgCu_2$ | 0.7350 | – | – | | [23] |
| $YFe_{10}Cr_2$ | $I4/mmm$ (No. 139) | $ThMn_{12}$ | 0.8415 | – | 0.4733 | | [9] |
| $Y_3(Fe,Cr)_{29}$ | $A2/m$ (No. 12) | $Nd_3(Fe,Ti)_{29}$ | 1.0645 | 0.8455 | 0.9678 | 97.462° | [10] |

dispersive spectroscopy (EDS) and optical microscopy were used for microstructural analysis. For the electron probe microanalysis and metallographic analysis of the samples, standard techniques were used. The metallographic samples were etched by a solution containing 1% HF, 3% $HNO_3$ and 96% $H_2O$.

## 3. Results and discussion

### 3.1. Phase analysis

Four binary compounds, i.e. $Y_2Fe_{17}$, $Y_6Fe_{23}$, $YFe_3$ and $YFe_2$ and a ternary compound $YFe_{10}Cr_2$ in the Y–Fe–Cr ternary systems have been confirmed to exist at 773 K by analyzing the XRD patterns of the binary and ternary samples. The XRD patterns of these compounds basically corresponded with the respective PDF data or the diffraction patterns calculated from the crystallographic data available in literature by using the PowderCell program [25] or lazy program.

In order to verify the existence of the σ phase at 773 K, a series of alloy samples with the composition of near FeCr were prepared. The XRD analysis results of the binary alloy samples indicated that all the samples consisted of the phases of Fe and Cr pointing to the absence of the σ phase at 773 K. The XRD analysis on the ternary alloy samples with composition near FeCr also pointed out that the σ phase is absent at 773 K. This is in good agreement with that reported in Refs. [26,27]. No binary compound was observed in the Y–Cr system at 773 K.

A series of samples with composition near $YFe_{10}Cr_2$ were prepared to confirm the existence of the ternary compound $YFe_{10}Cr_2$. The ternary compound of $YFe_{10}Cr_2$ with a tetragonal $ThMn_{12}$-type structure was confirmed to exist at 773 K. It was found that there are some homogeneity range in $YFe_{12-x}Cr_x$ with $x = 2.1$–$3.4$ at 773 K. That is to say the homogeneity range of the phase $YFe_{12-x}Cr_x$ extended from about 16 at.% Cr to 26 at.% Cr at 773 K. Fig. 1 presents the XRD pattern of sample No. 155 with the single phase of $YFe_{12-x}Cr_x$ ($x = 2.5$).

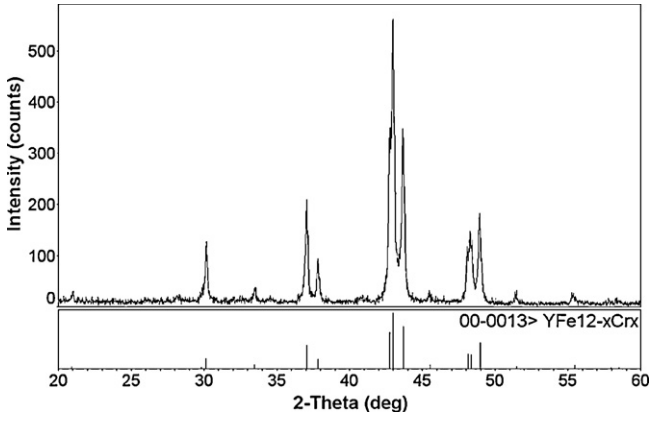


**Fig. 1.** The XRD pattern of sample No. 155 with the single phase of $YFe_{12-x}Cr_x$ ($x = 2.5$).

In order to verify the existence of $Y_3(Fe,Cr)_{29}$ at 773 K, four samples with the compositions $Y_3Fe_{29-x}Cr_x$ ($x = 3.0$, 4.0, 5.0, 6.0) were prepared. The as-cast samples were subsequently annealed in a sealed quartz tube for 10 days at 1273 K, and then quenched in liquid nitrogen. The XRD patterns of these samples corresponded with the XRD data of $Y_3(Fe,Cr)_{29}$ calculated from the crystallographic data available in literature [10,28] showing the existence of the phase $Y_3(Fe,Cr)_{29}$ in the samples. The samples were re-annealed in an evacuate quartz tube at 1173 K for 30 days, cooled down to 773 K at a rate of 50 K/day and kept for more than 10 days. The XRD analysis indicated that the samples consisted of the phases of $Y_2Fe_{17-x}Cr_x$ and $YFe_{12-x}Cr_x$ without the phase $Y_3(Fe,Cr)_{29}$ in the samples. This means that the phase $Y_3(Fe,Cr)_{29}$ in the samples was absent and had decomposed into the two phases of $Y_2Fe_{17-x}Cr_x$ and $YFe_{12-x}Cr_x$ at 773 K. This pointed to that the phase $Y_3(Fe,Cr)_{29}$ is a high temperature phase, which is in accordance with the results of the Refs. [11,18,26,28]. Fig. 2 is the micrograph of the sample No. 177 with composition $Y_3Fe_{29-x}Cr_x$ with $x = 5.0$ (annealed at 1173 K for 30 days and 773 K for 10 days). The sample contained the two phases of $Y_2Fe_{17-x}Cr_x$ and $YFe_{12-x}Cr_x$ without the phase of $Y_3(Fe,Cr)_{29}$ reported by Refs. [10,28]. In Fig. 2, the background with composition of $Y_{10.4}Fe_{71.2}Cr_{18.4}$ is $Y_2Fe_{17-x}Cr_x$ and the light grey pieces with composition of $Y_{8.8}Fe_{68.8}Cr_{22.4}$ are $YFe_{12-x}Cr_x$. No new ternary and binary compound was found in the system.

### 3.2. Solid solubility

The solid solubilities of Cr in the compounds $Y_2Fe_{17}$, $Y_6Fe_{23}$, $YFe_3$ and $YFe_2$ were determined by X-ray diffraction technique using the phase-disappearing and lattice parameter method combined with the SEM (EDS). By comparing the movement of the diffraction pat-

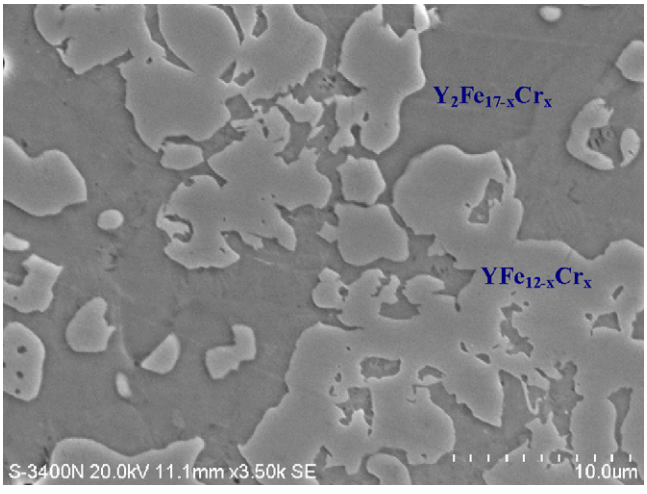


**Fig. 2.** Micrograph of sample No. 177 with composition $Y_3Fe_{29-x}Cr_x$ with $x = 5.0$ (annealed at 1173 K for 30 days and 773 K for 10 days). The background is $Y_2Fe_{17-x}Cr_x$ and the light grey pieces are $YFe_{12-x}Cr_x$.

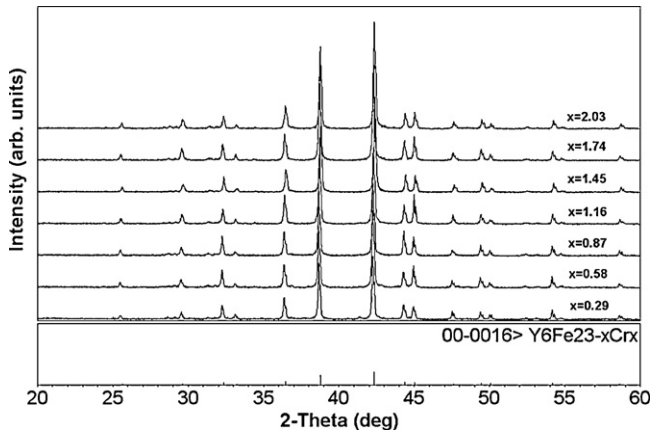


**Fig. 3.** The XRD patterns of the samples with composition of $Y_6Fe_{23-x}Cr_x$ ($x$ = 0.29, 0.58, 0.87, 1.16, 1.45, 1.74, 2.03).

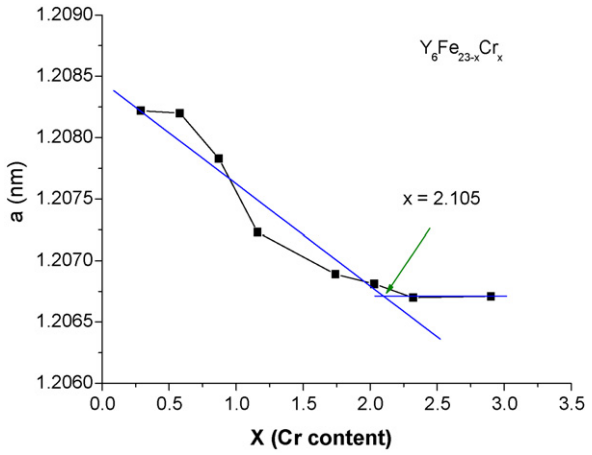


**Fig. 4.** Variation of the lattice parameters of $Y_6Fe_{23-x}Cr_x$ with the content of Cr.

terns of the single phases and the disappearance of the phases, the solid solubilities of Cr in these compounds were roughly obtained. The lattice parameters of samples containing Cr and/or compounds $Y_2Fe_{17-x}Cr_x$, $Y_6Fe_{23-x}Cr_x$, $YFe_{3-x}Cr_x$ and $YFe_{2-x}Cr_x$ were also calculated and refined from XRD patterns by using the computer Software Jade 5.0 and the least square method to determine the solubilities of Cr in these compounds. The SEM (EDS) was also applied to observe the solubilities of the compounds. Fig. 3 presents the XRD patterns of the samples $Y_6Fe_{23-x}Cr_x$ ($x$ = 0.29, 0.58, 0.87, 1.16, 1.45, 1.74, 2.03). It can be seen clearly from Fig. 3 that these samples contained the single phase of $Y_6Fe_{23-x}Cr_x$ pointing to the maximum solid solubility of Cr in $Y_6Fe_{23-x}Cr_x$ is around 7 at.% Cr ($x$ = 2.03). Analysis by lattice parameter method gave the same result. Fig. 4 shows the variation of the lattice parameters of $Y_6Fe_{23-x}Cr_x$ with the content of Cr obtained by the computer Software Jade 5.0 and the least square method. Further analysis by the SEM (EDS) also showed that the maximum solid solubility of Cr in $Y_6Fe_{23}$ is 6.0 at.% Cr. Fig. 5 is the micrograph of the sample No. 65 with composition $Y_{28.6}Fe_{68.6}Cr_{2.8}$ in the phase region of $Y_6Fe_{23-x}Cr_x + YFe_{2-x}Cr_x + YFe_3$. The grey strip-shape phase with composition of $Y_{33.7}Fe_{61.3}Cr_{5.0}$ is $YFe_{2-x}Cr_x$, the grey bulge background with composition of $Y_{25.8}Fe_{72.9}Cr_{1.3}$ is $YFe_3$ and the grey pieces with composition of $Y_{21.2}Fe_{72.8}Cr_{6.0}$ are $Y_6Fe_{23-x}Cr_x$. The Rietveld refinements for the solid solution $Y_6Fe_{23-x}Cr_x$ were carried out by using the DBWS9411 program [29]. The Rietveld refinement results indicated that the maximum solid solution of Cr in $Y_6Fe_{23-x}Cr_x$ is 6 at.% Cr ($x$ = 1.74). Table 2 presents the Rietveld refinement results of the compounds $Y_6Fe_{23-x}Cr_x$ ($x$ = 0.58, 1.16, 1.74, 2.03, 2.32). The Rietveld refinement of the sample No. 162 ($Y_6Fe_{23-x}Cr_x$, $x$ = 2.03) pointed to that the sample contained a small amount of $YFe_{12-x}Cr_x$ and $Y_2Fe_{17-x}Cr_x$ except the main phase of $Y_6Fe_{23-x}Cr_x$. There are 93.8 wt.% $Y_6Fe_{23-x}Cr_x$, 4.9 wt.% $Y_2Fe_{17-x}Cr_x$ and 1.1 wt.% $YFe_{12-x}Cr_x$ in the sample. The lattice parameters of these phases were refined to be of $a$ = 1.20737(1) nm for $Y_6Fe_{23-x}Cr_x$, $a$ = 0.8587(5) nm and $c$ = 0.4776(3) for $YFe_{12-x}Cr_x$, and of $a$ = 0. 8462(2) nm and $c$ = 0.8283(3) nm for $Y_2Fe_{17-x}Cr_x$. The Rietveld refinements for the solid solution $Y_6Fe_{23-x}Cr_x$ also pointed out that the substitutions of Cr atoms for Fe prefer to partially occupy the 4b and 24d sites ($Cr_{0.5}Fe_{0.95}$ at 4b and $Cr_{0.329}Fe_{0.671}$ at 24d for the sample No. 162) in the solid solution phase $Y_6Fe_{23-x}Cr_x$. Table 3 lists the Rietveld refined atomic parameters and isotropic temperature factors for the sample No. 162 ($Y_6Fe_{23-x}Cr_x$, $x$ = 2.03).

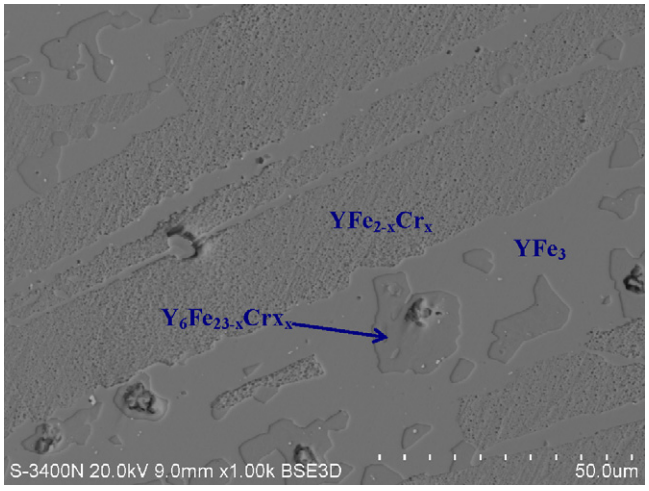


**Fig. 5.** The micrograph of the sample No. 65 with composition of $Y_{28.6}Fe_{68.6}Cr_{2.8}$. The grey strip-shape phase is $YFe_{2-x}Cr_x$, the grey bulge background is $YFe_3$ and the grey pieces are $Y_6Fe_{23-x}Cr_x$.

**Table 2**
Rietveld refinement results of the compounds $Y_6Fe_{23-x}Cr_x$ ($x$ = 0.58, 1.16, 1.74, 2.03, 2.32).

| Cr content, $x$ | Phases | Space group | Lattice parameters (nm) | | | Weight fraction (%) | Reliability factors | | |
|---|---|---|---|---|---|---|---|---|---|
| | | | $a$ | $b$ | $c$ | | $R_p$ | $R_{wp}$ | $R_{exp}$ |
| 0.58 | $Y_6Fe_{23-x}Cr_x$ | $Fm\bar{3}m$ | 1.20776(1) | | | 100 | 0.110 | 0.145 | 0.051 |
| 1.16 | $Y_6Fe_{23-x}Cr_x$ | $Fm\bar{3}m$ | 1.20770(2) | | | 100 | 0.109 | 0.136 | 0.047 |
| 1.74 | $Y_6Fe_{23-x}Cr_x$ | $Fm\bar{3}m$ | 1.20765(1) | | | 100 | 0.114 | 0.147 | 0.051 |
| 2.03 | $Y_6Fe_{23-x}Cr_x$ | $Fm\bar{3}m$ | 1.20737(1) | | | 93.8 | 0.106 | 0.136 | 0.051 |
| | $YFe_{12}$ | $I4/mmm$ | 0.8587(5) | | 0.4776(3) | 1.1 | | | |
| | $Y_2Fe_{17}$ | $P6_3/mmc$ | 0. 8462(2) | | 0.8283(3) | 4.9 | | | |
| 2.32 | $Y_6Fe_{23-x}Cr_x$ | $Fm\bar{3}m$ | 1.20742(1) | | | 81.2 | 0.103 | 0.136 | 0.050 |
| | $YFe_{12}$ | $I4/mmm$ | 0.84641(4) | | 0.47939(4) | 10.0 | | | |
| | $Y_2Fe_{17}$ | $P6_3/mmc$ | 0.84607(3) | | 0.82894(4) | 8.8 | | | |

**Table 3**
Rietveld refined atomic parameters and isotropic temperature factors for the compound $Y_6Fe_{23-x}Cr_x$ ($x$ = 2.03).

| Atoms | Sites | $x$ | $y$ | $z$ | Occupancy | $B_{eq}$ |
|---|---|---|---|---|---|---|
| M1 (M = Fe,Cr) | 4b | 1/2 | 1/2 | 1/2 | $Cr_{0.5}Fe_{0.95}$ | 0.1743 |
| M2 | 24d | 0 | 1/4 | 1/4 | $Cr_{0.329}Fe_{0.671}$ | 0.9637 |
| Y | 24e | 0.2030(1) | 0 | 0 | 1 | 0.3713 |
| Fe3 | 32f | 0.3782(1) | 0.3782(1) | 0.3782(1) | 1 | 0.6240 |
| Fe4 | 32f | 0.1772(1) | 0.1772(1) | 0.1772(1) | 1 | 0.3574 |

Fig. 6 presents the observed, calculated and differential X-ray powder diffraction patterns for the sample No. 162 ($Y_6Fe_{23-x}Cr_x$, $x$ = 2.03). The $R$-factors of the Rietveld refinement for the sample No. 162 are $R_p$ = 0.106 and $R_{wp}$ = 0.136, respectively.

Similarly, the maximum solid solubilities of Cr in $Y_2Fe_{17}$ and $YFe_2$ were determined to be 18 and 6 at.% Cr at 773 K, and the maximum solid solubilities of Cr in Fe and Fe in Cr were about 13 at.% Cr and 15 at.% Fe, respectively. The homogeneity range in the ternary compound $YFe_{12-x}Cr_x$ was found to be about $x$ = 2.1–3.4 at 773 K. The samples No. 183 and No. 184 with compositions of $Y_{25}Fe_{74}Cr_1$ and $Y_{25}Fe_{73}Cr_2$ were prepared to determine the solid solubility of Cr in $YFe_3$. The X-ray diffraction analysis pointed out that both the samples contained the same three phases of $Y_6Fe_{23-x}Cr_x$, $YFe_{2-x}Cr_x$ and $YFe_3$. No solubility of Cr in $YFe_3$ is observed at 773 K.

### 3.3. Isothermal section of the Y–Fe–Cr system at 773 K

The isothermal section of the phase diagram of the Y–Fe–Cr ternary system at 773 K has been studied by using the X-ray diffraction technique, optical microscopy, differential thermal analysis, scanning electron microscopy equipped with energy dispersive spectroscopy analysis. By comparing and analyzing a total of 188 binary and ternary alloy samples and identifying the phases in each sample, the 773 K isothermal section of the phase diagram of the Y–Fe–Cr ternary system is obtained. The isothermal section consists of 8 single-phase regions, 14 two-phase regions and 7 three-phase regions, seen in Fig. 7. The typical alloys and the details of the three-phase regions of the isothermal section of the Y–Fe–Cr ternary system are given in Table 4.

Fig. 8 presents the XRD pattern of the equilibrated sample No. 42 ($Y_{20.0}Fe_{46.0}Cr_{34.0}$) consisting of the three phases of $YFe_{12-x}Cr_x$, $YFe_{2-x}Cr_x$ and Cr and proving the existence of the three-phase region of $YFe_{12-x}Cr_x + YFe_{2-x}Cr_x + Cr$. The microstructure of the sample No. 179 ($Y_{9.4}Fe_{68.7}Cr_{21.9}$) examined by SEM clearly showed the existence of the three phases of $YFe_{12-x}Cr_x$, $Y_2Fe_{17-x}Cr_x$ and $Y_6Fe_{23-x}Cr_x$, seen in Fig. 9. The grey background with composition of $Y_{8.7}Fe_{66.6}Cr_{24.7}$ is the phase $YFe_{12-x}Cr_x$, the

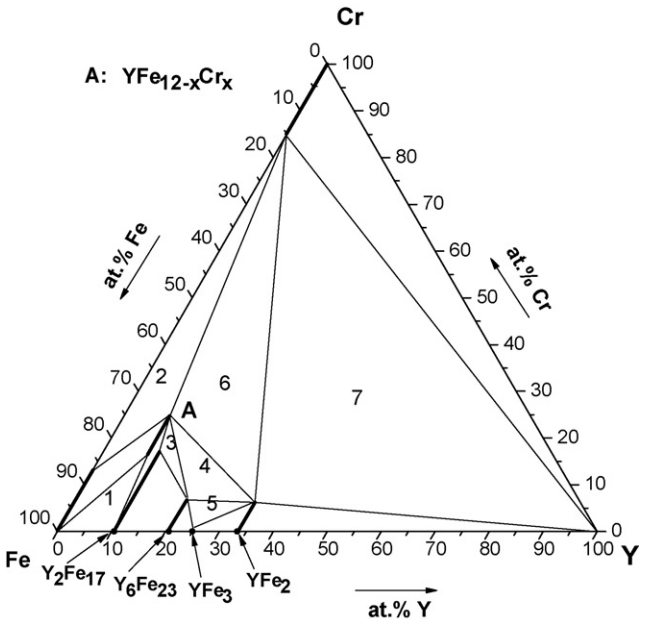


**Fig. 7.** Isothermal section of the phase diagram of the Y–Fe–Cr ternary system at 773 K.

**Table 4**
Details of the typical alloys and phase components in three-phase regions.

| Phase regions | Alloy compositions | Phase components |
|---|---|---|
| 1 | $Y_{9.4}Fe_{87.5}Cr_{3.1}$ | $\alpha$-Fe + $Y_2Fe_{17-x}Cr_x$ + $YFe_{12-x}Cr_x$ |
| 2 | $Y_{5.2}Fe_{69.8}Cr_{25.0}$ | $\alpha$-Fe + $YFe_{12-x}Cr_x$ + Cr |
| 3 | $Y_{9.4}Fe_{68.7}Cr_{21.9}$ | $Y_2Fe_{17-x}Cr_x$ + $YFe_{12-x}Cr_x$ + $Y_6Fe_{23-x}Cr_x$ |
| 4 | $Y_{24.1}Fe_{68.8}Cr_{7.1}$ | $YFe_{12-x}Cr_x$ + $Y_6Fe_{23-x}Cr_x$ + $YFe_{2-x}Cr_x$ |
| 5 | $Y_{28.6}Fe_{68.6}Cr_{2.8}$ | $Y_6Fe_{23-x}Cr_x$ + $YFe_{2-x}Cr_x$ + $YFe_3$ |
| 6 | $Y_{20.0}Fe_{46.0}Cr_{34.0}$ | $YFe_{12-x}Cr_x$ + $YFe_{2-x}Cr_x$ + Cr |
| 7 | $Y_{25.1}Fe_{19.8}Cr_{55.1}$ | $YFe_{2-x}Cr_x$ + Cr + $\alpha$-Y |

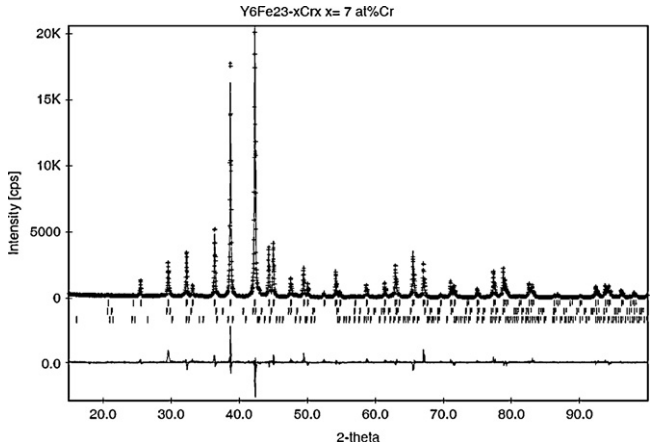


**Fig. 6.** The observed, calculated and differential X-ray powder diffraction patterns for the sample No. 162 ($Y_6Fe_{23-x}Cr_x$, $x$ = 2.03).

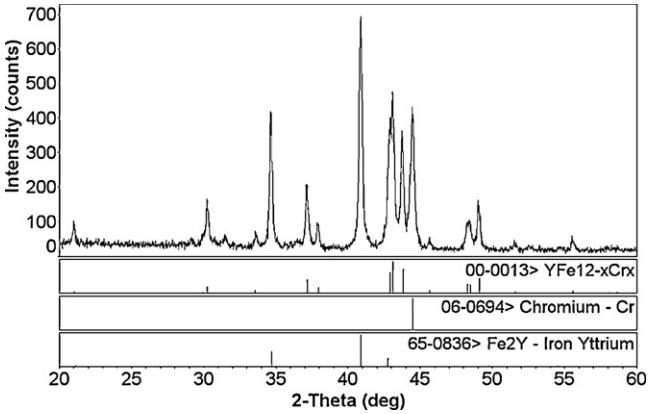


**Fig. 8.** The XRD pattern of the sample No. 42 ($Y_{20.0}Fe_{46.0}Cr_{34.0}$) containing the three phases of $YFe_{12-x}Cr_x$, $YFe_{2-x}Cr_x$ and Cr.

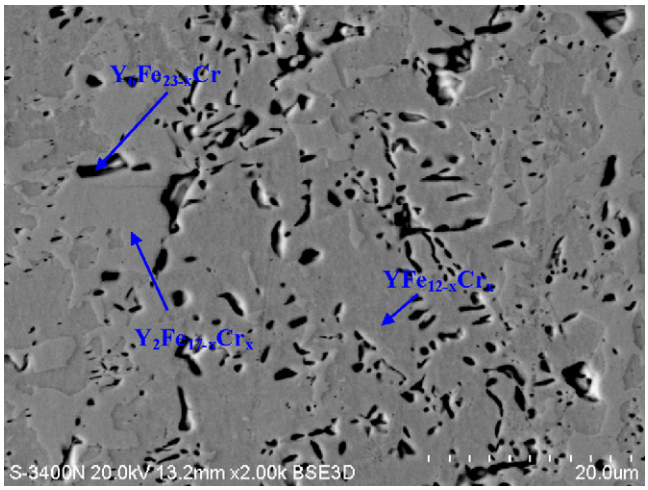


**Fig. 9.** The SEM micrograph of the sample No. 179 ($Y_{9.4}Fe_{68.7}Cr_{21.9}$) indicated the existence of the three-phase region of $YFe_{12-x}Cr_x + Y_2Fe_{17-x}Cr_x + Y_6Fe_{23-x}Cr_x$. The grey background is the phase $YFe_{12-x}Cr_x$, the bright grey bulge pieces are $Y_2Fe_{17-x}Cr_x$ and the black pieces are the phase $Y_6Fe_{23-x}Cr_x$.

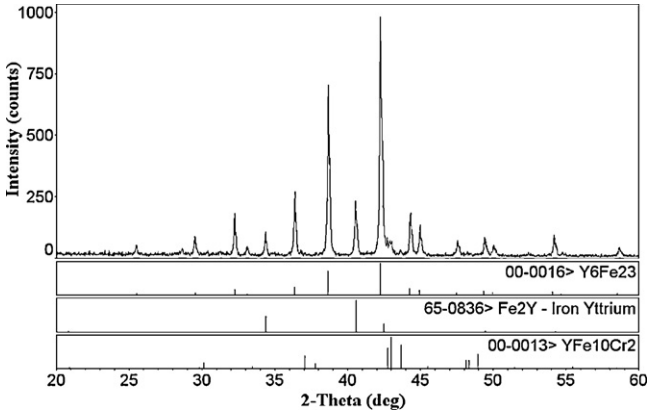


**Fig. 10.** The XRD pattern of the sample No. 72 ($Y_{7.1}Fe_{68.8}Cr_{24.1}$) consisting of the three phases of $Y_6Fe_{23-x}Cr_x$, $YFe_{12-x}Cr_x$ and $YFe_{2-x}Cr_x$.

bright grey bulge pieces with composition of $Y_{10.9}Fe_{68.9}Cr_{20.2}$ are $Y_2Fe_{17-x}Cr_x$ and the black pieces are the phase $Y_6Fe_{23-x}Cr_x$. The XRD pattern of the sample No. 72 ($Y_{7.1}Fe_{68.8}Cr_{24.1}$) located in the three-phase region of $Y_6Fe_{23-x}Cr_x + YFe_{12-x}Cr_x + YFe_{2-x}Cr_x$ is given in Fig. 10, indicating the existence of the three-phase region of $Y_6Fe_{23-x}Cr_x + YFe_{12-x}Cr_x + YFe_{2-x}Cr_x$.

## 4. Conclusion

The phase relations of the Y–Fe–Cr ternary system at 773 K has been determined by using X-ray powder diffraction, optical microscopy, differential thermal analysis, scanning electron microscopy equipped with energy dispersive spectroscopy techniques. The isothermal section consists of 8 single-phase regions, 14 two-phase regions and 7 three-phase regions. Four binary compounds and one ternary compounds were confirmed to exist in the system at 773 K. The maximum solid solubilities of Cr in Fe, $Y_2Fe_{17}$, $Y_6Fe_{23}$ and $YFe_2$ is 13, 18, 6 and 6 at.% Cr, respectively. The maximum solid solubility of Fe in Cr is about 15 at.% Fe. There are some homogeneity range in the unique ternary compound of $YFe_{12-x}Cr_x$ in the system with $x = 2.1–3.4$ (from 16 at.% Cr to 26 at.% Cr) at 773 K. No solubility of Cr in $YFe_3$ is observed at 773 K. The ternary compound of $Y_3Fe_{29-x}Cr_x$ was not observed at 773 K. No new ternary and binary compound was found in the system.

## Acknowledgements

This work was supported by the Natural Science Foundation of China (Nos. 50861005 and 50961002), the Special Foundation for the New Century Talents Program of Guangxi (No. 2007217) and Natural Science Foundation of Guangxi (No. 0832027).

## References

[1] Y.C. Yang, B. Kebe, W.J. James, J. Appl. Phys. 52 (3) (1981) 2077–2078.
[2] J.J. Bara, B.F. Bogacz, A.Z. Pedziwiatr, P. Stefanski, A. Szlaferek, A. Wzeciono, J. Alloys Compd. 265 (1998) 70–76.
[3] C.P. Yang, Y.Z. Wang, B.P. Hu, J.L. Wang, Z.X. Wang, Z.L. Jiang, C.L. Ma, J. Zhu, J. Alloys Compd. 290 (1999) 144–149.
[4] F.R. de Boer, Z.G. Zhao, K.H.J. Buschow, J. Magn. Magn. Mater. 157/158 (1996) 504–507.
[5] B. Garcia-Landa, D. Fruchart, D. Gignoux, J.L. Soubeyroux, R. Vert, J. Magn. Magn. Mater. 182 (1998) 207–215.
[6] R. Vert, D. Fruchart, B. Garcia-Landa, D. Gignoux, Y. Amako, J. Alloys Compd. 275–277 (1998) 611–614.
[7] O. Moze, K.H.J. Buschow, J. Alloys Compd. 233 (1996) 165–168.
[8] P. Qian, N.X. Chen, J. Shen, Solid State Commun. 134 (2005) 771–776.
[9] F.M. Yang, Q.A. Li, R.W. Zhao, J.P. Kuang, F.R. de Boer, J.P. Liu, K.V. Rao, G. Nicolaides, K.H.J. Buschow, J. Alloys Compd. 177 (1991) 93–100.
[10] C.P. Yang, Y.Z. Wang, G.H. Wu, X.F. Han, B.P. Hu, C.L. Ma, X.Y. Chen, J. Zhu, J. Phys.: Condens. Matter 11 (1999) 6843–6849.
[11] H.S. Li, J.M. Cadogan, R.L. Davis, A. Margarian, J.B. Dunlop, Solid State Commun. 90 (1994) 487–492.
[12] C.P. Yang, Y.Z. Wang, G.H. Wu, B.P. Hu, J. Du, X.F. Han, J.L. Wang, Z.L. Jiang, J. Zhu, Solid State Commun. 111 (1999) 247–252.
[13] X.F. Han, H.L. Liu, E.J. Jin, M. Ishizone, M. Oogane, H. Kato, J. Magn. Magn. Mater. 282 (2004) 206–210.
[14] V. Psycharis, M. Gjoka, C. Christides, D. Niarchos, J. Alloys Compd. 317–318 (2001) 455–458.
[15] D.P. Lazar, M. Valeanu, A. Galatanu, M.R. Leonovici, A. Dafinei, L. Ion, J. Alloys Compd. 392 (2005) 31–39.
[16] B.P. Hu, G.C. Liu, Y.Z. Wang, B. Nasunjilegal, N. Tang, F.M. Yang, H.S. Li, J.M. Cadogan, J. Phys.: Condens. Matter 6 (1994) L595–L599.
[17] F.M. Yang, B. Nasunjilegal, J.L. Wang, H.Y. Pan, W.D. Qing, R.W. Zhao, B.P. Hu, Y.Z. Wang, G.C. Liu, H.S. Li, J.M. Cadogan, J. Appl. Phys. 76 (1994) 1971–1973.
[18] O. Kalogirou, V. Psycharis, L. Saettas, D. Niarchos, J. Magn. Magn. Mater. 146 (1995) 335–345.
[19] J. Yang, S.Z. Dong, W.H. Mao, P. Xuan, Y.C. Yang, Physica B 205 (1995) 341–345.
[20] T.B. Massalski, H. Okamoto, P.R. Subramanian, L. Kacprzak, Binary Alloy Phase Diagrams, ASM International, Materials Park, 1990.
[21] O. Kubaschewski, Phase Diagram of Binary Fe-based Systems, Spinger-Verlag/Verlag Stahleisen mbH, Berlin, Heidelberg/Dusseldorf, 1982.
[22] V.P. Itkin, in: H. Okamoto (Ed.), Phase Diagrams of Binary Iron Alloys, ASM International, Materials Park, OH, 1993, pp. 102–129.
[23] P. Villars, Pearson's Handbook of Crystallographic Data, ASM International, Materials Park, OH, 1997.
[24] Materials Data JADE Release 5.0, XRD Pattern Processing, Materials Data Inc., Livermore, CA, 2002.
[25] W. Kraus, G. Nolze, J. Appl. Crystallogr. 29 (1996) 301–303.
[26] Q.R. Yao, H.L. Wang, Z.W. Liu, H.Y. Zhou, S.K. Pan, J. Alloys Compd. 475 (2009) 286–288.
[27] Y. Ustinovshikov, B. Pushkarev, J. Alloys Compd. 389 (2005) 95–101.
[28] Z. Hu, W.B. Yelon, Solid State Commun. 91 (1994) 223–226.
[29] A.R. Young, User's Guide to Program DBWS-9411 for Rietveld Analysis of X-ray and Neutron Powder Diffraction Patterns, School of Physics, Georgia Institute of Technology, Atlanta, GA, 1995.